Analytical Grid Generation for accurate representation of clearances in CFD for Screw Machines

S Rane, A Kovačević and N Stošić

City University London, Centre for Positive Displacement Compressor Technology, London, UK.
Email: sham.rane.1@city.ac.uk

Abstract. One of the major factors affecting the performance prediction of twin screw compressors by use of computational fluid dynamics (CFD) is the accuracy with which the leakage gaps are captured by the discretization methods. The accuracy of mapping leakage flows can be improved by increasing the number of grid points on the profile. However, this method faces limitations when it comes to the complex deforming domains of a twin screw compressor because the computational time increases tremendously. In order to address this problem, an analytical grid distribution procedure is formulated that can independently refine the region of high importance for leakage flows in the interlobe space. This paper describes the procedure of analytical grid generation with the refined mesh in the interlobe area and presents a test case to show the influence of the mesh refinement in that area on the performance prediction. It is shown that by using this method, the flow domains in the vicinity of the interlobe gap and the blow-hole area are refined which improves accuracy of leakage flow predictions.

1. Introduction

The CFD analysis of the working chamber of a screw machine is transient in nature and requires a grid which could accurately represent the deformation of the domain. In this respect, algebraic methods are convenient for quick adjustment and recalculation of the grid. *Kovačević, Stošić* and *Smith* [1, 2] have successfully used an algebraic grid generation method together with boundary adaptation and transfinite interpolation which has been implemented in program SCORG – Screw Compressor Rotor Grid Generator. *Sauls* and *Branch* [6] have applied SCORG to achieve results from CFD calculations in order to develop an improved one-dimensional thermodynamic model for refrigeration screw compressors by extracting calibration coefficients that influence the pressure variation during the discharge process. *Pascu et al*. [7] have reported optimization of the discharge port of a Twin screw compressor using SCORG grid generator. Optimization was based on the selection of the port geometry by relative comparison of flow field predicted by the CFD models. *Nouri et al*. [8] have carried out cycle-resolved velocity measurements within a screw compressor using LDV and these data have been used by *Kethidi et al*. [9] to compare with the results from 3D CFD models.

Voorde, Vierendeels and *Dick,* [10] have implemented a grid conversion algorithm for unstructured to block structured mesh from solution of Laplace equation for twin screw compressors and pumps using the differential methods. Based on this grid generation, flow in a double tooth compressor and a twin screw compressor has been analyzed and the results have been compared with experimental data over a range of discharge pressure and rotor speeds.

Recently CFX Berlin has introduced a software tool called TwinMesh to generate numerical mesh for ANSYS CFX solver. This tool generates grid for twin rotor machines on similar principles as that of

the algebraic and differential approaches. *Hesse et al*. [11] have presented the application of such a deforming grid for the analysis of an oil free twin screw compressor.

Only limited studies are available on prediction of leakage flows using 3D CFD models. *Kovačević* and *Rane* have reported in [3] results from the analysis of a dry air expander and it was found that CFD models deviated in prediction of leakage flow much more under the operating condition of low rotor speed and higher pressure difference then at higher rotor speeds with low pressure difference. On the other hand, *Rane et al*. in [4] analyzed a twin screw compressor at one discharge pressure and one rotor speed and found that refinement of the rotor grid in circumferential direction has a direct influence on the prediction of the mass flow rate. However, pressure and power prediction showed lower sensitivity to grid refinement. In another study, *Kovačević et al.* [5] compared the predictions from two different CFD solution approaches and it was found that there is a big influence of the type of solver used for calculations on the prediction of leakage flows through the compressor. Again a low impact was found on the pressure and power prediction accuracy.

One of the major factors affecting the performance prediction of twin screw compressors by use of computational fluid dynamics is the accuracy with which the leakage gaps are captured by the discretization methods. In order to represent rotor profiles accurately, it is required to use point definition of the geometry but this definition gets compromised when a numerical grid is generated for flow calculations. One of the methods of improving the profile accuracy is by increasing the number of grid points on the profile. However, this method faces limitations when it comes to the complex deforming computational domain of the twin screw compressor because the grid quality deteriorates and computational time increases tremendously.

In order to address this problem, an analytical grid distribution procedure has been proposed in this paper that can independently refine the region of high importance i.e. the interlobe space. To achieve this, a new procedure is used for generation of the initial point distribution on compressor boundaries. This procedure uses equidistant distribution of points on the outer boundary of the domain which consists of the casing and rack to calculate distribution on rotors. By this means it is possible to refine mesh in the interlobe gap to allow for a more accurate prediction of leakage flows. The total grid size can be controlled by limiting the number of cells in the region not containing interlobe gap and blow-hole areas. The paper presents the principle of this analytical grid generation and a test case to demonstrate the influence of interlobe refinement on the performance prediction. A direct influence of interlobe grid refinement on leakage flow prediction has been verified from the study. This type of grid coupled with real time clearance variation procedure would be required in future to produce more reliable and accurate predictions from CFD analysis of screw machines.

2. Analytical grid generation for refinement of the interlobe numerical mesh

The rotor flow domain is divided into two subdomains belonging to two rotors using the rack plane which can be generated analyticaly or numerically using Willis meshing conditions [1]. Following that the main steps of mesh generation in each cross section are:

- Outer boundary in each block is defined as a combination of the rack segment and the casing circle segment. The rack segment stretches between the bottom CUSP point to the top CUSP point and is closed by the casing as shown in Figure 2.
- Rack segment is discretized using equidistant distribution. It is possible to use same distribution for both subdomains in order to maintain conformal interface if required.
- Casing segment in each subdomain is discretized using equidistant distribution which is usually different than for the rack segment. The distribution obtained on the outer boundaries of the two blocks is the reference for the rotor profile distribution.
- Nodes are distributed on the rotor profile with corresponding distribution available on the outer boundary. It is very likely that at first the initial cells will overlap for helical rotors, especially on the face of the gate rotor profile.
- Distribution on rotor profiles is regularized using background blocking.
- Interior nodes are distributed using transfinite interpolation [1].

- Orthogonalisation and smoothing iterations are performed to improve cell quality [1].

Most of the steps listed above are described earlier in [1]. Therefore only the background blocking is described in this paper. It can be considered as a uniform distribution of nodes on the rotor profile and on the outer circle as shown in Figure 1.

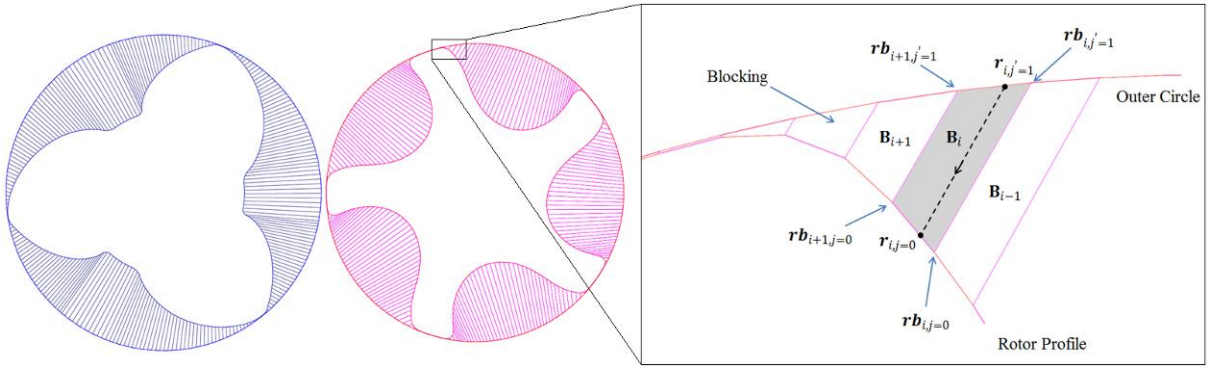

Figure 1. Background blocking for the main and gate rotors

The advantage of such blocks is that:

- Blocks do not have to be as refined as the final grid.
- Blocks can be used as reference for refinement in any required regions.
- Blocks have to be calculated only once and simply rotate for various rotor positions.

Suppose that the points distributed on the boundaries are represented in index notation with respect to the physical coordinate system as $\boldsymbol{r}_{i,j}\,(x,y)$. Points on the rotor profile are $\boldsymbol{r}_{i,j=0}\,(x,y)$, points on the outer boundary consisting of casing and rack curve are $\boldsymbol{r}_{i,j=1}\,(x,y)$ and the point distribution on outer full circle is $\boldsymbol{r}_{i,j'=1}\,(x,y)$. Each of the background blocks is identified by its index $\boldsymbol{B}_i$. The points on the inner boundary of the blocks which are the rotor profile nodes are $\boldsymbol{rb}_{i,j=0}\,(x,y)$ and the point distribution on outer full circle is $\boldsymbol{rb}_{i,j'=1}\,(x,y)$ as shown in Figure 1.

Starting from the bottom CUSP, nodes are distributed on the outer circle covering the rack part with required number of points i_{rack}. Nodes are then distributed on the outer circle covering the casing part with required number of points i_{casing}. At this stage the data are available for $\boldsymbol{rb}_{i,j=0}\,(x,y)$, $\boldsymbol{rb}_{i,j'=1}\,(x,y)$ and $\boldsymbol{r}_{i,j'=1}\,(x,y)$ and it is required to calculate $\boldsymbol{r}_{i,j=0}\,(x,y)$. This node distribution is based on equidistant spacing as given in equation 1.

$$\boldsymbol{r}_{i,j'=1}(x,y) = \boldsymbol{r}_{i-1,j'=1}(x,y) + S_i\, i \tag{1}$$

$$S_i = \frac{S_\mathrm{I}}{\mathrm{I}}$$

$$S_I = \boldsymbol{r}_{I,j'=1}(x,y) - \boldsymbol{r}_{i=0,j'=1}(x,y)$$

A scanning function is introduced that has the information of the background blocking. Starting from the bottom CUSP, the scanning function traces each node $\boldsymbol{r}_{i,j'=1}\,(x,y)$ and identifies the block $\boldsymbol{B}_i$ to which it belongs. There can be situation when a single block has multiple nodes present in it or there can be blocks with no nodes present. This is because the distribution on the rack curve can be refined in comparison to the blocking. Similarly the distribution on the casing can be coarse in comparison with the blocking. Once the nodes associated with each block are traced by the scanning function, an arc-length based projection is used to determine the nodes $\boldsymbol{r}_{i,j=0}\,(x,y)$ to be placed on the rotor profile. At the same time constraint is imposed on the node placement that they have to be bound in the same block $\mathbf{B}_i$ $\boldsymbol{B}_i$ as that of the outer circle nodes $\boldsymbol{r}_{i,j'=1}\,(x,y)$.

Figure 1 shows the projection of $\boldsymbol{r}_{i,j'=1}(x,y)$ on the inner boundary of the block in order to get $\boldsymbol{r}_{i,j=0}(x,y)$. This projection is based on arc length factor given by equation 2.

$$\boldsymbol{r}_{i,j=0}(x,y) = \boldsymbol{rb}_{i,j=0}(x,y) + \left(\boldsymbol{rb}_{i+1,j=0}(x,y) - \boldsymbol{rb}_{i,j=0}(x,y)\right)\frac{S_i}{S_I} \quad (2)$$

$$S_i = \boldsymbol{r}_{i,j'=1}(x,y) - \boldsymbol{rb}_{i,j'=1}(x,y)$$
$$S_I = \boldsymbol{rb}_{i+1,j'=1}(x,y) - \boldsymbol{rb}_{i,j'=1}(x,y)$$

The calculated positions $\boldsymbol{r}_{i,j=0}(x,y)$ of nodes ensure that they are guided by a regular rotor profile. Regularised distribution is superimposed onto the rack curve by finding the intersection points of the distribution lines and the rack curve. These intersection points are the new distributions $\boldsymbol{r}_{i,j=1}(x,y)$on the rack curve as shown in Figure 2.

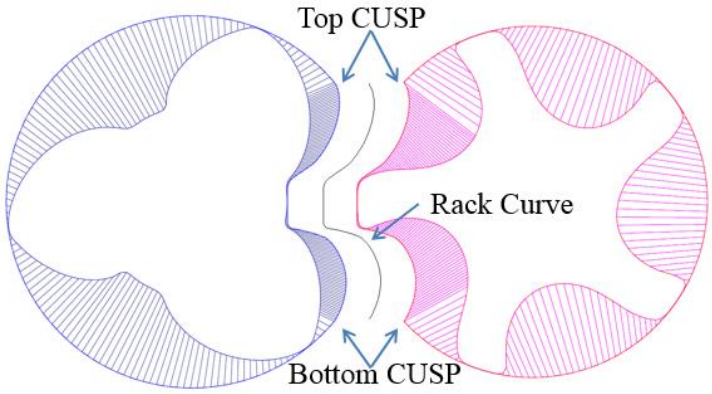

Figure 2. Refinement in the rack segment and superimposition of rack curve

Since the blocks on the main rotor side are different from the blocks on the gate rotor side, the intersection points obtained on the common rack curve from the two blocks are not identical. This results in a non-conformal map between the two rotor blocks. But this implementation gives an important feature to the grid to be able to construct refinement in the interlobe region. This region is important for capturing the rotor profile in the leakage gap and hence has strong influence on the leakage flow calculation from the solution. As an example, the cross section mesh with interface regions is highlighted and the three dimensional grid with helical lobes is shown in Figure 3. The mesh in the cross sections results in all quadrilateral cells with independent settings applicable for the number of nodes in the interlobe region. With the blocking approach the 3D grid is fully hexahedral and both the main and the gate rotor surfaces are smoothly captured. At the transition point from interlobe region to the casing region small non-aligned node movements are possible. However, these are positioned on the surface of the rotors and do not result in any irregular cells. The surface mesh on the casing is of the highest quality with regular quadrilateral cells. The surface mesh on the interlobe interface mostly follows axial grid lines with only small transverse movements in the vicinity of the top and bottom CUSP's which are cyclically repeating. These movements are on the surface of the interface and do not result in any irregular cells. The current implementation allows for a fully conformal interface with the equal index of the top and bottom CUSP points which ensures straight line in the axial direction. This accurately captures blow-hole area as shown in Figure 4.

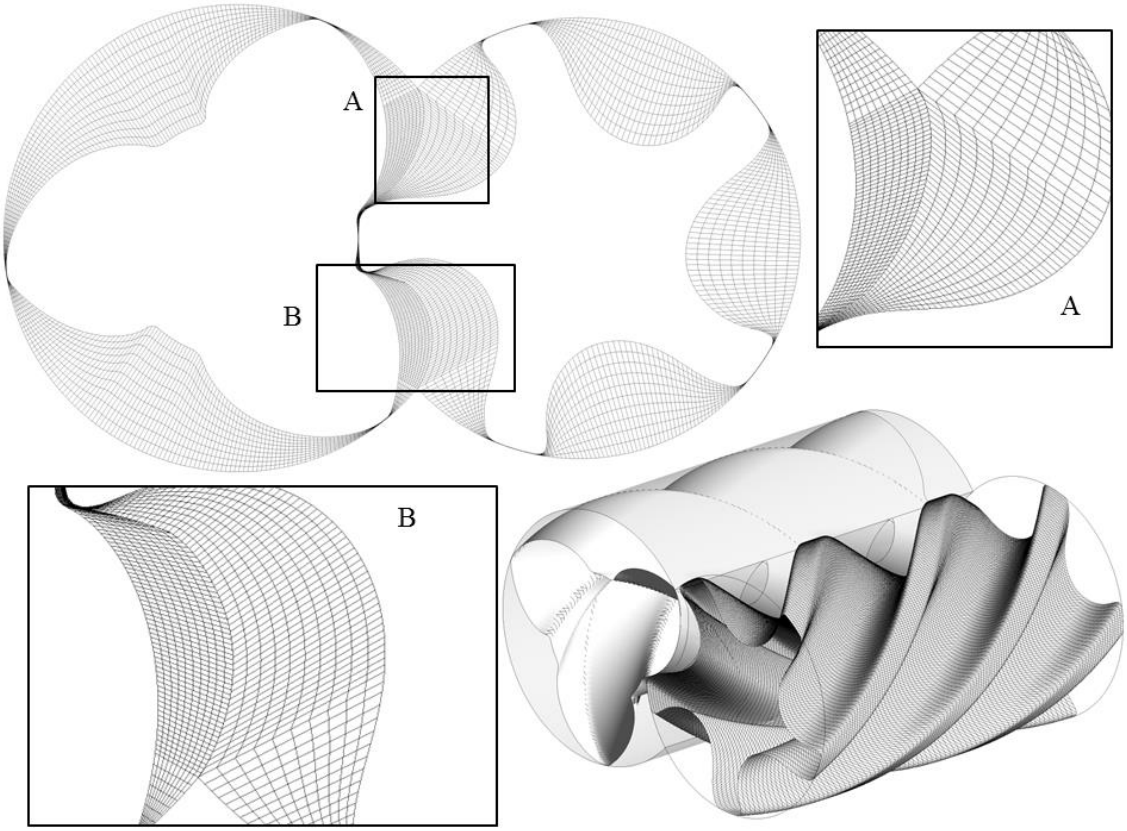

Figure 3. Grid generated with background blocking in screw compressor rotor

Modern rotor profiles usually feature small radii, as for example in the root of the main and the tip of the gate rotor. If the grid distribution starts from the rotor profile to the casing [1], the grid lines on the rotors follow the helix and capture these small radii accurately. However, when the grid distribution starts from the casing to the rotor profile, the grid lines in axial direction are connecting nodes with same circumferential indices in consecutive cross sections, hence they do not run along the helix of the rotors. This results in some faces becoming warped in these areas as shown in Figure 4. However, the cells remain regular and very low effect on the flow regime in this area is recorded.

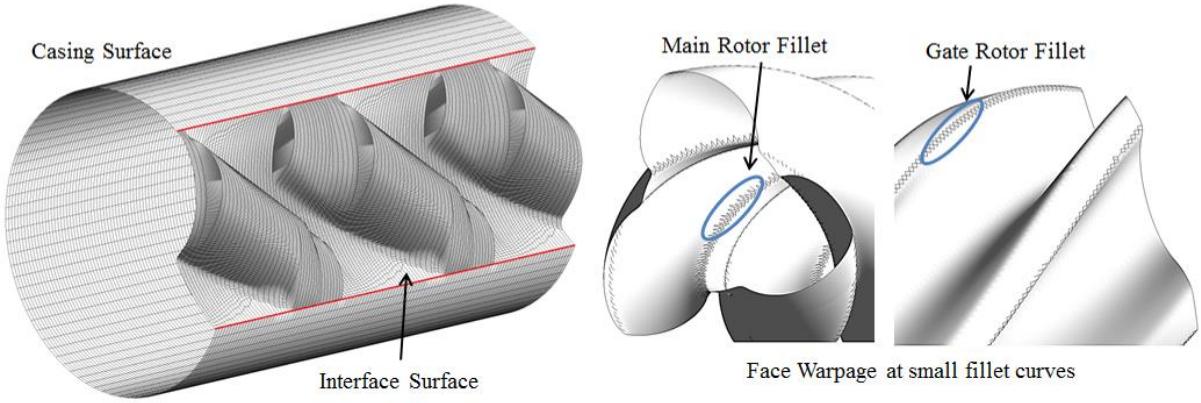

Figure 4. Surface mesh on the rotor, casing and the rack interface

3. Case study – Influence of interlobe grid refinement

An oil-free twin screw compressor with a 3/5 lobe arrangement of 'N' rotor profile rotors is modelled in this study. The male rotor diameter is 127.45 mm; the female rotor diameter is 120.02 mm while the centre distance between the two rotors is 93.00 mm. The length to diameter ratio of the rotors is 1.6 and the male rotor has a wrap angle 285.0 deg. The nominal interlobe, radial and end leakage gaps are 160 micro meters each. The built-in volume index of the compressor is 1.8.

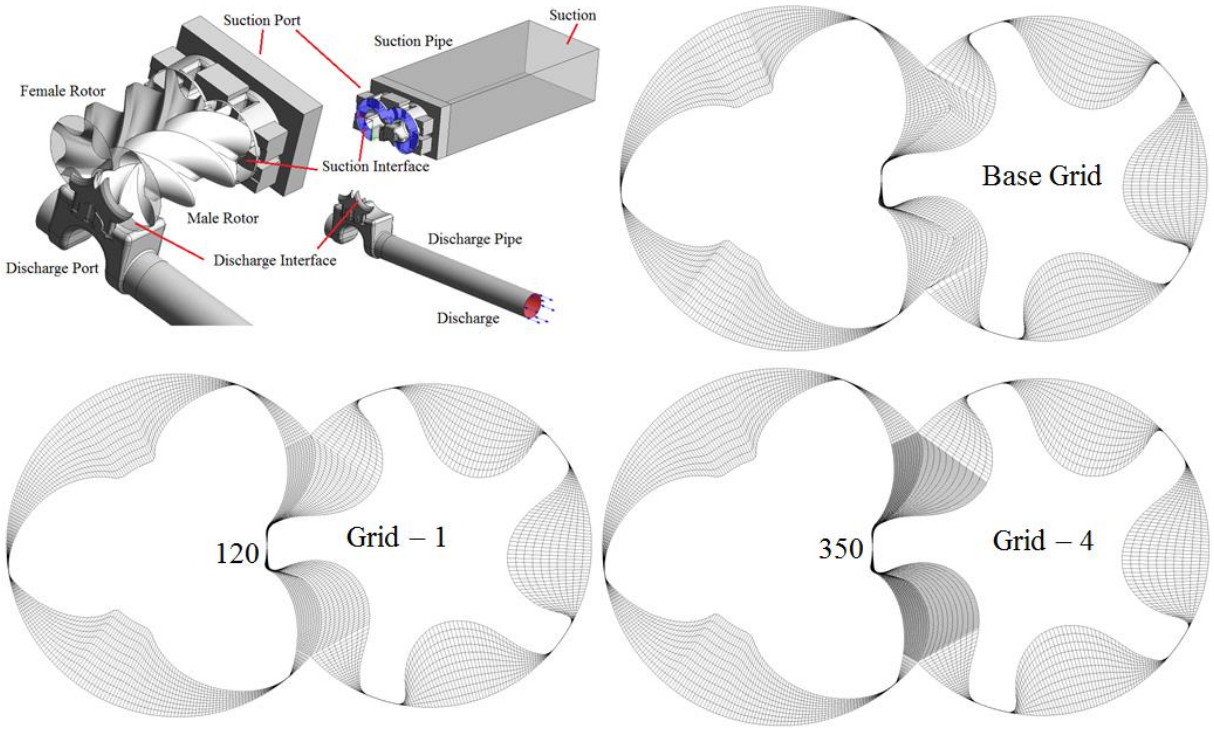

Figure 5. CFD Model Domain and Grid refinements in the interlobe clearance

Table 1. Grid levels and number of divisions.

Level	**Circumference**	**Radial**	**Angular**	**Interlobe**	**Outer Circle**	**Mesh Size in Rotors**
Base Grid	70	10	50		260	913682
Grid – 1	72	10	50	120	240	942480
Grid – 2	80	10	50	150	250	1049818
Grid – 3	90	10	50	200	250	1178100
Grid – 4	120	10	50	350	250	1570800

During operation, the rotors are subjected to thermal deformation which changes the clearance gap size. CFD models used in the study do not take into consideration such changes in clearances. Therefore, it is estimated that the clearances will reduce with the increase in temperature and the grids for CFD are generated with reduced uniform clearances of 60 micro meters in the interlobe and radial gaps in order to compensate for thermal distortions [5]. The axial end clearances are not included in the CFD model. Figure 5 shows the CFD model domain, boundaries and the sample grid in the cross section of the rotor domain. The working fluid is air with molar mass of 28.96 kg/kmol, Specific Heat Capacity $1.0044e^{03}$ J/kg K, Dynamic Viscosity $1.831e^{-05}$ kg/m s and Thermal Conductivity $2.61e^{-02}$ W/m K. A uniform pressure of 1.0bar was specified at the suction while the discharge pressure is 2.0bar. The main rotor

speed was 6000rpm and 8000rpm. High resolution scheme was used in the ANSYS CFX solver and cycle average mass balance between the rotor suction and discharge was achieved within 1% in all cases. Four levels of interlobe refinement have been generated with the new grid such that the first level has a refinement comparable to that of the base grid. The refinement is only on the profile in the interlobe space and on the casing side the number of divisions has been maintained equivalent to that of the base grid. Table 1 shows the different grid levels used for calculations and cross section mesh is shown in Figure 5. The grid in port domains was tetrahedral with 300736 nodes and constant in all the cases. On an Intel i7, 3.0GHz processor with 16Gb RAM each calculation took about 36hrs computational time for 5 cyclic repetitions of flow conditions. The experimental layout is shown in Figure 6.

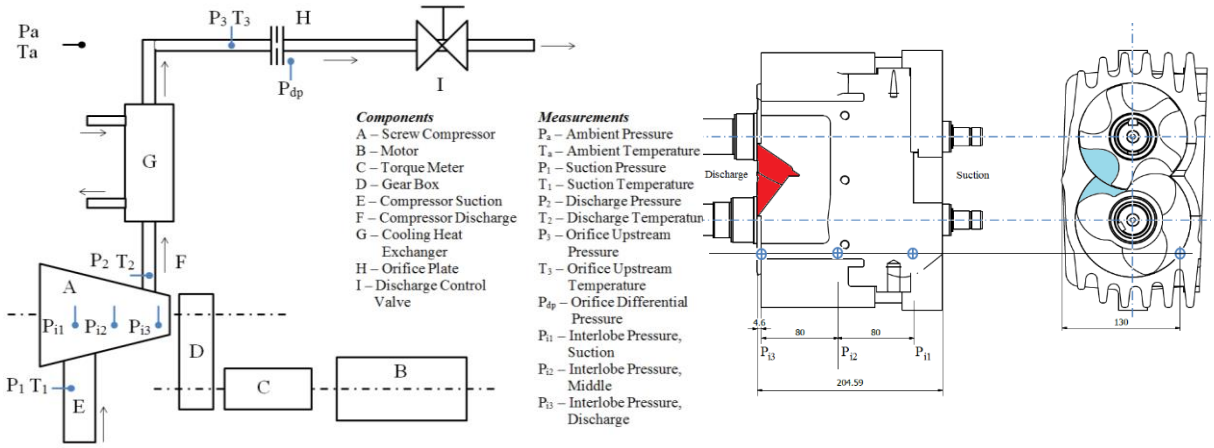

Figure 6. Layout of the test rig and location of the interlobe pressure transducers

3.1. Results and Discussion

The results from the analysis have been presented as a comparison of the internal pressure rise, indicated power (P_i), flow rate, volumetric efficiency (η_{vol}) and specific indicated power (P_{sp}) between the Base grid case and the various refinement levels of the new grid. Figure 7 is a plot of the pressure contour on the rotor surface with the two different grids. The surface of the rotor with Base grid is much regular as compared with the new grid but the pressure contour shows similar variation in both the cases.

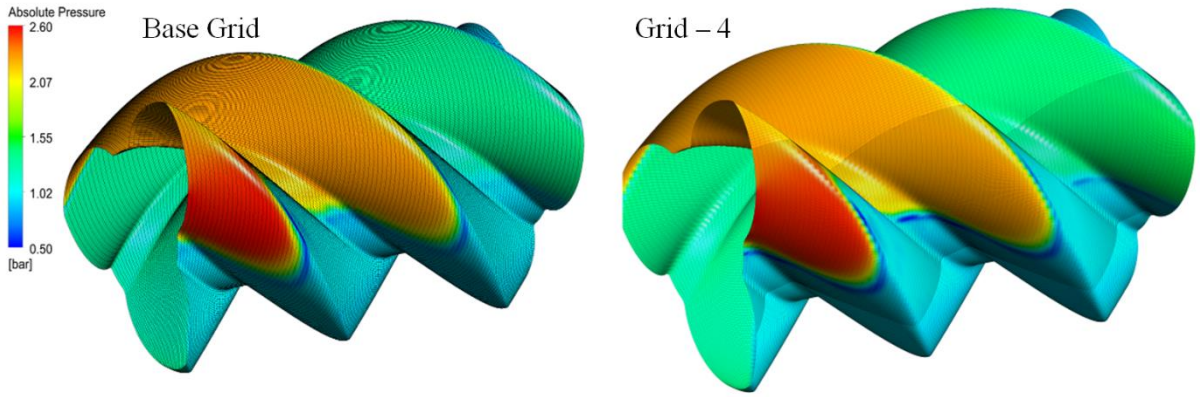

Figure 7. Pressure contours on the rotor surface with Base grid and Grid – 4, 8000rpm

3.2. Pressure – Angle variation

The interlobe pressure were measured using three pressure transducers mounted on the casing as shown in Figure 6. Pressure data from CFD results were obtained at the same coordinates as a cyclic average. Figure 8 shows the variation of pressure in the compression chamber at 6000rpm and 8000rpm. The plots from Base grid and new grids have been compared with experimental results. The internal pressure increase predicted by the base grid and new grids are very close to each other. Only a small increase in the compression rate is observed with the new Grid – 4. The pressure curves obtained by CFD are close to the experimentally obtained pressures, but the peak pressures from CFD models are slightly lower than experimental peak pressures at both 8000rpm and 6000rpm. Since the difference between the CFD and experimental peak pressures increases with speed, it is concluded that the thermal effects have big influence on the leakage gaps and further account of this phenomena will be necessary for better performance predictions. At the discharge pressure of 2.0bar and the current size of the discharge port, overcompression is observed with pulsations in the port which are accurately predicted by CFD.

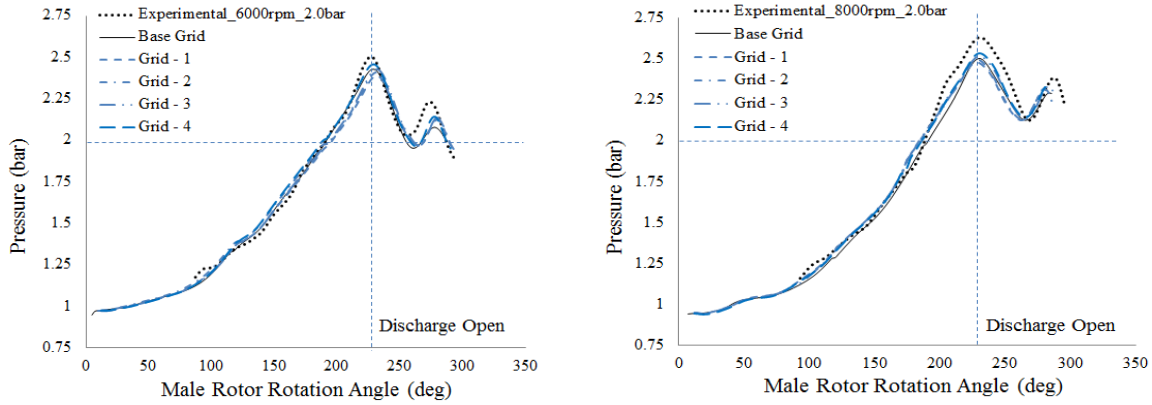

Figure 8. Pressure variation in the chamber with Male rotor rotation angle at 6000 and 8000rpm

3.3. Indicated Power.

Figure 9 shows the variation of the normalised indicates power (P_i) with speed for series of grid refinements. Predicted values and the experimental results of P_i have been normalized with respect to the indicated power obtained by the experiment. In order to extract the indicated power from measured power, it was assumed that the mechanical efficiency η_{mech} of the gearbox and bearings was constant at 95%. In reality it changes with speed and pressure ratio. The difference in P_i between CFD predictions on the base grid and the experiment is about –2.7% at 6000rpm and about –6.6% at 8000rpm. By using the new grid generation method, P_i is increasing at both speeds and all grid refinements getting closer to the measured values. The difference between CFD and experiment is about +1.4% at 6000rpm and about –2.8% at 8000 rpm with the finest Grid-4.

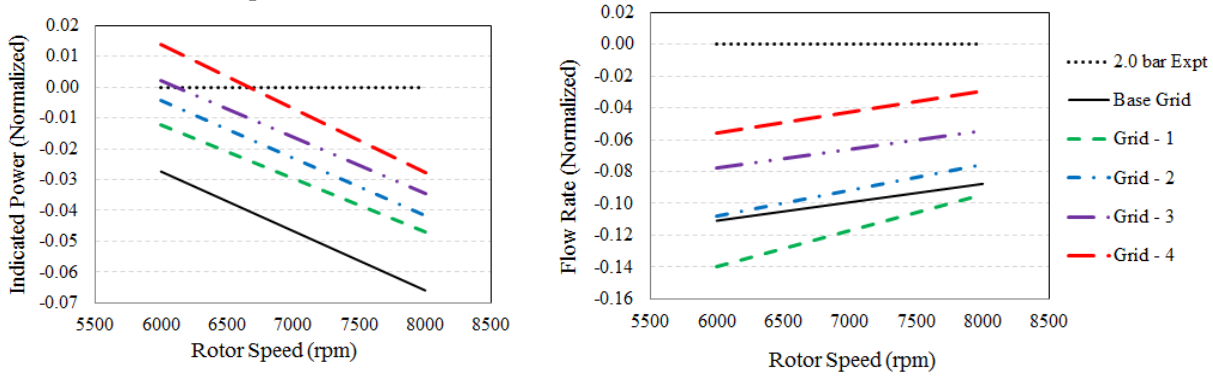

Figure 9. Comparison of Indicated power and Flow rate

3.4. Flow rate

Figure 9 shows the variation of the flow rate with speed with grid refinements. The predicted and measured flow rates are normalized with respect to the experimental results. The interlobe grid refinement has big influence on the flow rate. With the Base grid the difference between CFD prediction and experiment was about –11% at 6000rpm and –8.7% at 8000rpm. But this difference has strongly reduced with the Grid – 4 to –5.5% at 6000rpm and –2.9% at 8000rpm. The increase in flow rate also compares with the increase in P_i from Grid – 1 to Grid – 4.

The difference in flow rate prediction has reduced with interlobe refinement but it is still present. This is because the clearance gap of 60 micro meters has been assumed in the CFD model as the operating gap size. Due to thermal deformation and other operating uncertainties, the gap size is expected to vary. Few more iterations with reduced gap size could help in achieving further closer predictions from the model.

3.5. Volumetric efficiency

Figure 10 shows the variation of volumetric efficiency (η_{vol}) with speed for different grid refinements. The η_{vol} with Base grid is about 7% lower than the experiment. With new grid the difference is higher with Grid – 1 but reduces with further interlobe refinement. With Grid – 4 the difference in η_{vol} is just about 3% from the experiment. In line with the flow prediction, the difference is smaller at 8000rm as compared to that at 6000rpm.

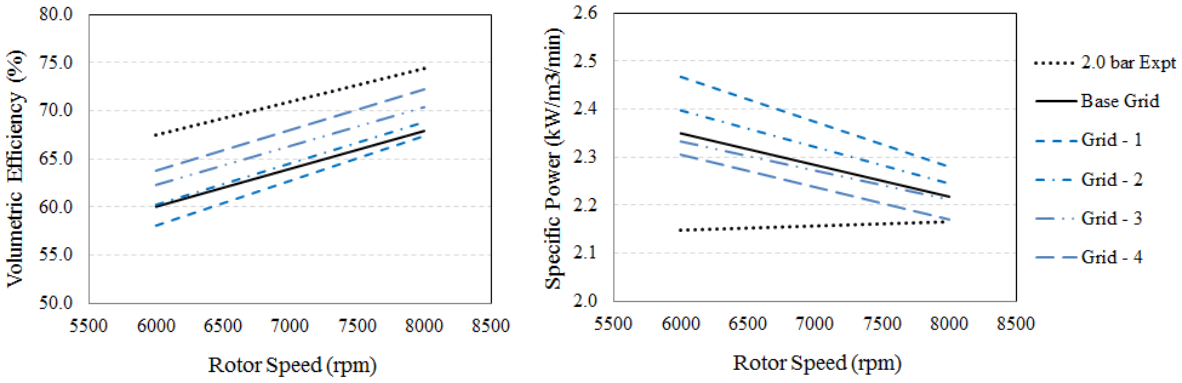

Figure 10. Comparison of Volumetric efficiency and Specific indicated power

3.6. *Specific Indicated Power.*

Figure 10 also shows the variation of specific indicated power (P_{sp}) with speed for different grid refinements. The P_{sp} is influenced by both the calculation of indicated power and the mass flow rate. With the Base grid specific indicated power is higher than experiment at both the speeds. The same trend is seen with the new grids because of the slight increase in indicated power as seen in Figure 9. From the level of Grid – 1 to Grid – 4 however this difference goes on reducing. At 6000rpm the difference between calculated and experimental P_{sp} is about 0.2 kW/m^3/min with Base grid and it has reduced to 0.15 kW/m^3/min with Grid – 4. At 8000rpm, the specific indicated power matches with the experiment with Grid – 4.

4. Conclusion

An algebraic grid generation procedure has been proposed for distribution of the boundary nodes in the grid generation of twin screw machines for CFD calculation. This distribution utilised the reference background blocking structure to identify nodes on the rotor profile based upon the nodes of the outer boundary. It allows the grid in the interlobe space to be refined and capture the rotor profile curvature

more accurately. The test case was presented which compares the CFD results with series of refined grids with experimental results.

- The grids generated by this procedure contain only quadrilateral cells with improved orthogonality. The interface between the rotors is non-conformal with much improved alignment which improves with the interlobe grid refinement. The method of 'outer-to inner' boundary grid generation causes the cells located in the tip and the root radii of the rotors to have larger warp angle compared to the traditional rotor to rack generated mesh.
- The interlobe grid refinement significantly improves the curvature of the rotor profiles, quality of the mesh and consequently the prediction of the mass flow rate and leakage flows.
- The interlobe grid refinement showed insignificant change in pressure history capture showing that in both cases the internal pressure curve was close to the experimental results.
- Indicated power increased by a small amount from Grid – 1 to Grid – 4 and was close to experimental value at both the speeds.
- A difference between CFD predictions and experimental results still exists. This can be attributed to the consideration of right operational clearance gaps in the CFD model.

In order to obtain higher accuracy in CFD predictions, the change in leakage gap sizes due to the thermal deformation needs to be accounted for in the CFD models. This requires employment of fluid-solid interaction modelling or using experimental data. The new grid generation approach however provides a flexibility to improve the resolution of the rotor geometry and thereby reduce inaccuracy in leakage flow calculations significantly.

References

[1] Kovačević A., 2005. Boundary Adaptation in Grid Generation for CFD Analysis of Screw Compressors, *Int. J. Numer. Methods Eng.,* Vol. **64**: 401-426.

[2] Kovačević A., Stošić N. and Smith I. K., 2007. *Screw compressors - Three dimensional computational fluid dynamics and solid fluid interaction*, ISBN 3-540-36302-5, Springer-Verlag Berlin Heidelberg New York.

[3] Kovačević A. and Rane S., 2013. 3D CFD analysis of a twin screw expander, *8th International conference on compressors and their systems*, London, p. 417.

[4] Rane S., Kovačević A., Stošić N. and Kethidi M., 2014. Deforming grid generation and CFD analysis of variable geometry screw compressors, Computers and Fluids, 99, p. 124–141.

[5] Kovačević A., Rane S., Stošić N., Jiang Y., Furmanczyk M. and Lowry S., 2014. Influence of approaches in CFD Solvers on Performance Prediction in Screw Compressors, *Proc. Int. Compressor Conf. at Purdue*, Paper 1124.

[6] Sauls J. and Branch S., 2013. Use of CFD to develop improved one-dimensional thermodynamic analysis of refrigerant screw compressors. 8th Int conf on compressors and their systems, p. 591.

[7] Pascu M., Kovačević A. and Udo N., 2012. Performance Optimization of Screw Compressors Based on Numerical Investigation of the Flow Behaviour in the Discharge Chamber. Proc. Int. Compressor Conf. at Purdue. Paper 1145.

[8] Nouri J. M., Guerrato D., Stošić N., Kovačević A., and Arcoumanis, C., 2006, Cycle-resolved velocity measurements within a screw compressor. Proc. Int. Compressor Conf. at Purdue, Paper 1810.

[9] Kethidi M., Kovačević A., Stošić N., Smith I. K., 2011. Evaluation of various turbulence models in predicting screw compressor flow processes by CFD. 7th Int conf on compressors and their systems, p. 347.

[10] Voorde Vande J., Vierendeels J., 2005. A grid manipulation algorithm for ALE calculations in screw compressors. *17th AIAA Computational Fluid Dynamics Conference*, Canada, AIAA 2005-4701.

[11] Hesse J., Spille-Kohoff A., Hauser J., Schulze-Beckinghausen P., 2014. Structured meshes and reliable CFD simulations: TwinMesh for positive displacement machines. International screw compressor conference, TU Dortmund.

[12] Stošić N., Smith I.K. and Kovačević A., 2005. *Screw Compressors: Mathematical Modeling and Performance Calculation*, Monograph, Springer Verlag, Berlin, June 2005, ISBN: 3-540-24275-9.